AUTHOR QUERY FORM

AIP Publishing	Journal: J. Appl. Phys. Article Number: 017642JAP	Please provide your responses and any corrections by annotating this PDF and uploading it according to the instructions provided in the proof notification email.

Dear Author,

Below are the queries associated with your article; please answer all of these queries before sending the proof back to AIP. Please indicate the following:
Figures that are to appear as color online only (i.e., Figs. 1, 2, 3) 1, 2, 3, 4 (this is a free service).
Figures that are to appear as color online and color in print________ (a fee of $325 per figure will apply).

Article checklist: In order to ensure greater accuracy, please check the following and make all necessary corrections before returning your proof.

1. Is the title of your article accurate and spelled correctly? Yes.
2. Please check affiliations including spelling, completeness, and correct linking to authors. We have checked it.
3. Did you remember to include acknowledgment of funding, if required, and is it accurate? We have checked it.

Location in article	Query / Remark: click on the Q link to navigate to the appropriate spot in the proof. There, insert your comments as a PDF annotation.
AQ1	Please check that the author names are in the proper order and spelled correctly. Also, please ensure that each author's given and surnames have been correctly identified (given names are highlighted in red and surnames appear in blue).
AQ2	We were unable to locate a digital object identifier (doi) for Refs. 5 and 26. Please verify and correct author names and journal details (journal title, volume number, page number, and year) as needed and provide the doi. If a doi is not available, no other information is needed from you. For additional information on doi's, please select this link: http://www.doi.org/.

Thank you for your assistance.

Answer to AQ1
We have checked it and they are correct.

Answer to AQ2
The information on publication year of Ref.5 was wrong. It should be "2008".
An author "D. Franta" should be added to Ref.26.

JOURNAL OF APPLIED PHYSICS **120**, 000000 (2016)

Propagation length of mid-infrared surface plasmon polaritons on gold: Impact of morphology change by thermal annealing

AQ1 Nobuyoshi Hiramatsu,[1,2] Fumiya Kusa,[1,3] Kotaro Imasaka,[1] Ikki Morichika,[1] Akinobu Takegami,[1,3] and Satoshi Ashihara[1,a)]

[1]*Institute of Industrial Science, the University of Tokyo, 4-6-1 Komaba, Meguro-ku, Tokyo 153-8505, Japan*
[2]*Department of Applied Physics, Faculty of Engineering, The University of Tokyo, 7-3-1 Hongo, Bunkyo-ku, Tokyo 113-8656, Japan*
[3]*Department of Applied Physics, Tokyo University of Agriculture and Technology, 2-24-16 Nakacho, Koganei, Tokyo 184-8588, Japan*

(Received 25 August 2016; accepted 20 October 2016; published online xx xx xxxx)

We studied the propagation length of surface plasmon polaritons (SPPs) at the gold/air interface in the mid-infrared range. We showed that SPPs propagate for a distance of about or above 10 mm at a wavelength of 10.6 μm, in good agreement with the value predicted from the dielectric constant of polycrystalline gold. We also demonstrated that a simple treatment of thermal annealing led to noticeable elongation of SPP propagation length, accompanied by increased grain size and decreased surface roughness. Quantitative evaluation of SPP propagation length, in correlation with material's morphology, is important in designing plasmonic devices and beneficial for understanding the mechanisms of SPP's losses that underlie electric-field enhancement. *Published by AIP Publishing.* [http://dx.doi.org/10.1063/1.4966934]

I. INTRODUCTION

Plasmonics in the mid-infrared (IR) range has gained increasing attention[1,2] because of possible applications to surface-enhanced spectroscopy,[3,4] chemical/bio sensing,[5] thermal radiation control,[6] optoelectronic circuit,[7,8] nonlinear light-matter interactions,[9] etc. Surface plasmons (SPs), including surface plasmon polaritons (SPPs) and localized surface plasmons (LSPs), can be excited at mid-IR wavelengths on various materials.[2] Here, the behaviors of SPs significantly vary according to the material where they are excited.[2]

SPs on highly doped semiconductors that have plasma frequencies in the mid-IR range are closely bound to the material surface, exhibiting wavelength shortening and large Ohmic loss at mid-IR wavelengths. Therefore, these materials are suited for subwavelength confinement. In contrast, SPs on noble metals that have plasma frequencies in the visible range are weakly bound to the material surface, exhibiting subtle wavelength shortening and small Ohmic loss at mid-IR wavelengths. Therefore, noble metals are suited for applications where any of small loss, long propagation length, and large electric-field enhancement is required.[2,10] Among noble metals, gold is an excellent plasmonic material because of its high metallic conductivity and superior chemical stability.[11]

The propagation length of SPPs is an important physical quantity[12,13] because it sets the available physical size of plasmonic devices in applications like sensors and optoelectronic circuits. It is also important as a direct measure of SPP's losses, which underlie the degree of electric-field enhancement achievable upon excitations of SPPs and LSPs. Electric-field enhancement plays key roles in many plasmonic applications.

SPPs decay by radiative damping and non-radiative damping. Radiative damping occurs by coupling with (or scattering into) free-propagating light and other SPP states. Non-radiative damping originates from scattering of free electrons by electrons, phonons, defects, impurities, crystallite grain boundaries, etc.[14] Here, we note that non-radiative damping ends up with Joule heating and, therefore, is often termed as the Ohmic loss.[12] Both radiative and non-radiative damping rates depend on the microscopic structure of materials. Therefore, evaluation of the SPP propagation length, together with characterization of material's morphology, helps us understand the loss mechanisms of SPPs.

The earlier studies reported the propagation length of mid-IR SPPs on polycrystalline metal films of gold,[15–17] silver,[16,17] and copper.[18,19] The reported values were, however, inconsistent with each other, and it was difficult to get deeper insights since material's morphology was not characterized. Nowadays, it is possible to characterize the morphology by a variety of scanning probe microscopy techniques. In recent publications, the propagation length of SPPs on gold at visible wavelengths[12] and dielectric function of gold[20,21] have been studied in correlation with the morphology observed by atomic force microscopy (AFM). There has been, however, no report on the propagation length of mid-IR SPPs on gold, with simultaneous characterization of morphology.

In this study, we experimentally measured the propagation length of SPPs at the gold/air interface at a mid-IR wavelength of 10.6 μm and correlated it with the morphology of gold. Here, we characterized the morphology by AFM, scanning electron microscopy (SEM), and electron backscatter diffraction (EBSD). We showed that SPPs propagate for a distance of about or above 10 mm, in agreement with the

[a)]Electronic mail: ashihara@iis.u-tokyo.ac.jp

value predicted from the dielectric constant of polycrystalline gold. Furthermore, we demonstrated that the SPP propagation length can be increased by a simple treatment of thermal annealing, accompanied by the increased grain size and suppressed surface roughness. In this study, we exploited surface-relief gratings as input/output couplers. Compared with the prism coupling,[18,19] the grating coupling does not suffer from contamination of collinear radiative components.[16,17] Compared with the edge coupling,[16,17] the grating coupling provides higher coupling efficiency and the resultant better signal-to-noise ratio.

II. DEVICE DESIGN AND FABRICATION

In order to measure the propagation length of SPPs, we designed a series of SPP waveguide devices. Each device consists of an input coupler, an SPP waveguide, and an output coupler. The input and output couplers are surface relief gratings made of gold. SPPs are excited at the input coupler from freely propagating light, propagate along the SPP waveguide, and are re-converted to freely propagating light at the output coupler, as illustrated in Fig. 1(a).

The input-output power ratio should be a product of light-SPP coupling efficiency, SPP propagation efficiency (or transmittance), and SPP-light coupling efficiency. Therefore, if the input/output coupling efficiencies are identical among all devices, we can deduce the propagation length (the distance that SPP power falls to $1/e$ of its initial value) by measuring the input-output power ratio for devices with different waveguide lengths. In the experiments, we assumed that the coupling efficiencies are identical among all devices and measured output optical power for each device, while keeping incident optical power constant.

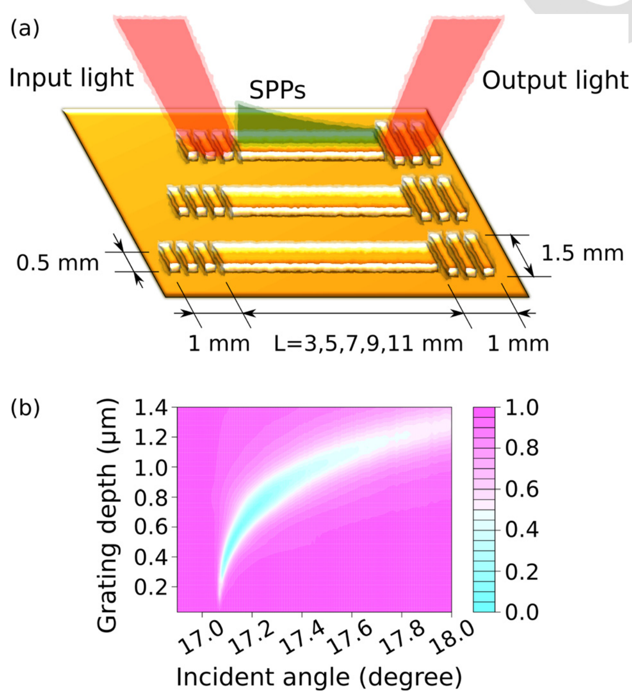

FIG. 1. (a) Schematic of the SPP waveguide devices. (b) Calculated reflection efficiency of a gold relief grating with a grating pitch of 15 μm and a duty cycle of 0.5, as a function of incident angle and grating depth.

Freely propagating light and SPPs can be coupled to each other by using a grating structure which satisfies the condition[22]

$$k_{\mathrm{SPPgr}} = k_0 \sin\theta + \frac{2m\pi}{d}, \tag{1}$$

where k_{SPPgr} and $k_0 = 2\pi/\lambda_0$ are the real parts of the complex wavenumber of the SPP at the grating and that of light in free space, respectively, λ_0 is the wavelength of light in free space, θ is an incident angle, d is a grating pitch, and m is an integer. Here, we note that k_{SPPgr} is close to the SPP wavenumber on a flat film in the case of shallow gratings.

Grating depth is known to be influential for the light-SPP (SPP-light) coupling efficiency.[22,23] To find the optimum grating depth for maximum coupling, we conducted numerical simulations on reflection efficiencies of surface relief gratings made of gold, by the rigorous coupled-wave analysis.[24]

Here, we assumed that each grating is made of polycrystalline gold and has a rectangular profile, a pitch of 15 μm, and a duty cycle of 0.5. Incident light was assumed to be a plane monochromatic wave at a wavelength of 10.6 μm. Figure 1(b) shows the calculated energy reflection efficiency as a function of incident angle and grating depth. The reflection efficiency reveals a dip at the grating depth of 0.2–1.3 μm and at the incident angle of 17°–18°. The energy loss in reflection is due to conversion from freely propagating light to SPPs. Considering the possible beam convergence of the incident light, we chose the grating depth of 0.8 μm for efficient coupling. Our choice is close to the conclusion derived by Cleary *et al.*[23] that the optimum grating depth of a rectangular grating was 10%–15% of the wavelength in the mid-IR range.

Physical dimensions of our devices are presented in Fig. 1(a). The SPP waveguides have a common width of 0.5 mm and varied lengths L of 3, 5, 7, 9, and 11 mm. The input (output) coupler is 1 mm in length and 0.5 mm (1.5 mm) in width. Both the input and output couplers have rectangular profiles with a grating pitch of 15 μm and a duty cycle of 0.5. The waveguides and the gratings were fabricated to have a common height of 0.8 μm from a gold base layer.

The devices were fabricated by means of electron beam lithography, thermal evaporation, and lift-off process. A gold base layer with a thickness of 200 nm was thermally evaporated on a silica glass substrate with a 5-nm-thick chromium adhesion layer, after the substrate was cleaned with acetone and ethanol. Then, the electron-beam resist (OEBR-CAP112PM, Tokyo Ohka Kogyo Co., Ltd) was spin-coated with a thickness of 1700 nm, exposed by electron beam, and developed. Finally, gold with a thickness of 800 nm was deposited on the developed resist, which was then lifted off by acetone. During the evaporation process, the substrate was not heated. The evaporation rate of gold was 0.4 nm/s, and the pressure inside the vacuum chamber was less than 4 mPa.

III. EXPERIMENT

Figure 2 shows the schematic of our experimental setup. A CO_2 laser (L3SL, Access Laser Company) was used as a

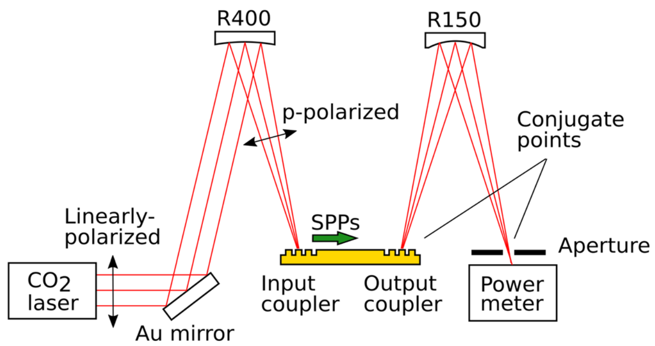

FIG. 2. Schematic of the experimental setup. R400 and R150 denote the spherical mirrors with curvature radii of 400 mm and 150 mm, respectively.

mid-IR light source generating linearly polarized light at a wavelength of 10.6 μm. Our SPP devices were attached to a rotational and 3D-translational stage. The p-polarized light (electric field lies within the plane of incidence) was incident onto the input coupler at the angle that fulfills Eq. (1) where $m = 1$, being loosely focused by a spherical mirror with a curvature radius R of 400 mm. Here, the incident light converged with an angle of 1.3° to form the beam spot of 0.6 mm diameter at the sample position. This plane-like wavefront of the incident light and the homogeneous grating coupler should result in a SPP beam with plane-like wavefront. Because the focal depth of the excited SPP beam is about 10 mm, and because the SPPs are confined in the waveguides, we ignored the propagation loss due to diffraction. The output light was collected by a spherical mirror of $R = 150$ mm and a power meter. An aperture was placed at the conjugate point of the output coupler to avoid any stray light. Time-averaged optical power sent to the input coupler was controlled to be 60 mW by adjusting the duty ratio of RF power modulation in the CO_2 laser.

In order to modify the morphology of the gold film, the sample containing a series of waveguide devices was annealed twice with a hotplate in an argon atmosphere.[25] In the first annealing process, the sample was heated at 600 °C for 20 min and gradually cooled down to room temperature on the hotplate. In the second annealing process, the sample was heated at 700 °C for 16 min and cooled down in the same way. The morphology was characterized by AFM (SPA-300, Seiko Instruments Inc.) in the tapping mode and by SEM/EBSD (JSM-6510LV, JEOL Ltd.) with the acceleration voltage of 20 kV.

IV. RESULTS

Figure 3 shows the measured output power as a function of the waveguide length L for as-grown, once-annealed (600 °C), and twice-annealed (600 °C and 700 °C) samples. Each trace was fitted with the exponential decay function $\exp(-L/L_{SPP})$ and normalized by the value at $L = 0$. Here, the propagation length L_{SPP} was evaluated to be 9.0 ± 0.3 mm, 12.0 ± 0.4 mm, and 14.7 ± 0.7 mm for the as-grown, once-annealed, and twice-annealed samples, respectively. In this way, the SPP propagation length was shown to increase noticeably by the thermal annealing treatment.

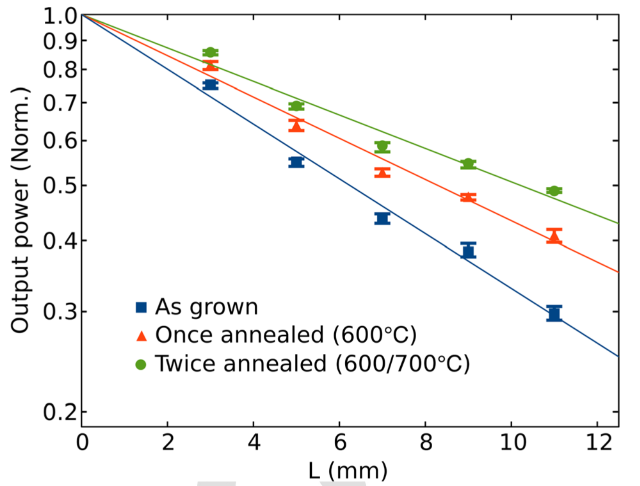

FIG. 3. Semi-logarithmic plot of normalized output power as a function of the SPP waveguide length L for the as-grown (squares), once-annealed (triangles), and twice-annealed (circles) samples. Exponential decay curves fitted to these data are also shown as solid lines. The propagation length of SPP was evaluated from each trace to be 9.0 ± 0.3 mm, 12.0 ± 0.4 mm, and 14.7 ± 0.7 mm.

Figure 4 shows an AFM topography image (upper panels) of the waveguide surface and the corresponding cross-sectional height data (lower panels) for (a) as-grown, (b) once-annealed (600 °C), and (c) twice-annealed (600 °C and 700 °C) samples. Here, the sectional surface is indicated as dashed lines in the topography images. It is evident from the cross-sectional height data that surface roughness was suppressed by the annealing treatment. By calculating root mean squares of deviations in height data, the surface roughness is estimated to be 5.7 nm, 2.8 nm, and 2.2 nm for the as-grown, once-annealed, and twice-annealed samples, respectively. The granular pattern typical for polycrystalline gold was clearly observed for the as-grown sample, as shown in Fig. 4(a). Here, we estimated the average diameter of crystallite grains to be 70 ± 20 nm for the as-grown sample, by analyzing the height data with the watershed algorithm[26] while assuming spherical shape for each grain. In contrast, grain boundaries were not identified for the annealed samples. We therefore proceeded to observe waveguide surface with SEM and EBSD.

Figure 4(d) shows a SEM image for the twice-annealed sample. It does not identify grain boundaries nor does the AFM topographic image shown in Fig. 4(c). Figure 4(e) shows the pattern quality map, constructed from the EBSD data, for the same sample and for the same area as shown in Fig. 4(d). Here, every point is assigned a brightness based on the EBSD pattern quality for that point. Bright area has high pattern quality (i.e., the measured electron diffraction pattern matches well with the ideal diffraction pattern of crystalline gold) and indicates crystalline gold. Dark area, in contrast, has low pattern quality and indicates grain boundaries, dislocations, and voids. The corresponding inverse pole figure (normal direction) is shown in Fig. 4(f) for reference. In this way, the granular pattern is successfully identified by the EBSD measurement. By analyzing the pattern quality data with the watershed algorithm,[26] while assuming spherical shape for each grain, we estimated the average diameter of

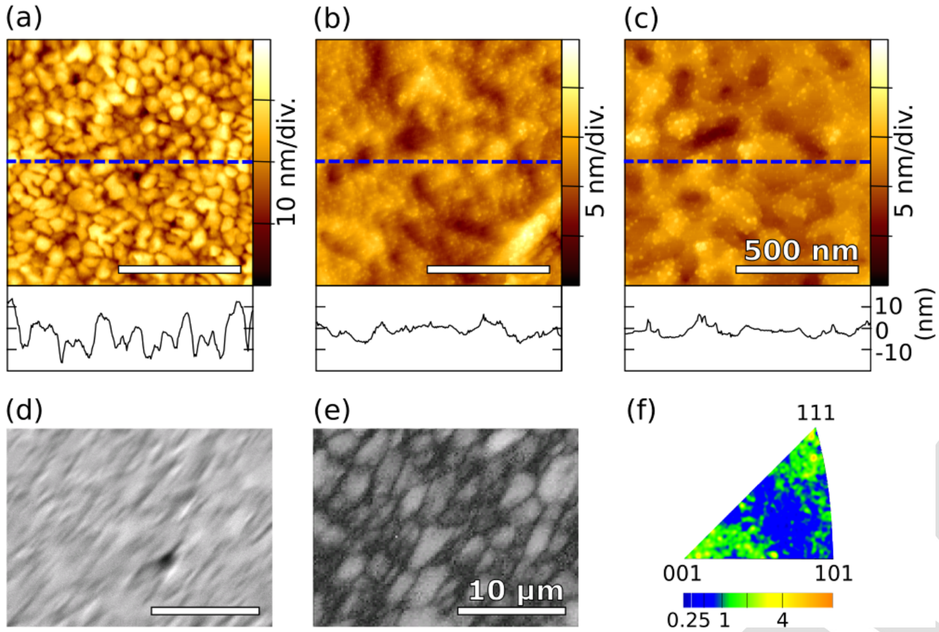

FIG. 4. AFM topography images (upper panels) of the waveguide surface and the corresponding cross-sectional height data (lower panels) for (a) as-grown, (b) once-annealed (600 °C), and (c) twice-annealed (600 °C and 700 °C) samples. The sectional surface is indicated as dashed lines. A SEM image, an EBSD pattern quality map, and an inverse pole figure for the twice-annealed sample are shown in (d), (e), and (f), respectively.

crystallite grains to be as large as $2 \pm 1\,\mu$m. In this way, thermal annealing at 700 °C or below was found to significantly increase the grain size and reduce the surface roughness.

The SPP-light coupling efficiency of the coupler was estimated to be 0.18 from our experiments. Although the optimum incident angle for the maximum coupling efficiency shifted by $\sim 0.5°$ upon annealing, the change in the maximum coupling efficiency was not observed. Additional AFM measurements confirmed that the coupler gratings had ideal rectangular profiles before and after the thermal annealing. This behavior is in contrast to the observation by Cleary *et al.*[23] that rectangular profiles of silver gratings became more sinusoidal after annealing. Such contrast may be caused by that their annealing temperature was closer to the melting point, compared with our case. Note that their annealing temperature of 840 °C was only about 122 °C lower than the melting point of silver (962 °C). In our case, the annealing temperature of 700 °C was about 364 °C lower than the melting point of gold (1064 °C).

V. DISCUSSIONS

In the following, we discuss the physics behind the elongation of the SPP propagation length upon thermal annealing, based on our observations of increased grain size (from 70 nm to 2000 nm) and suppressed surface roughness (from 5.7 nm to 2.2 nm).

Based on the Drude model, the complex dielectric constant of gold at frequency ω is expressed as

$$\tilde{\epsilon}(\omega) \equiv \epsilon' + i\epsilon'' = \epsilon_\infty - \frac{\omega_p^2}{\omega^2 + i\omega\omega_\tau} = \epsilon_\infty - \frac{\omega_p^2}{\omega^2 + \omega_\tau^2} + i\frac{\omega_p^2\omega_\tau}{\omega\left(\omega^2 + \omega_\tau^2\right)}, \qquad (2)$$

where ϵ' and ϵ'' are the real and imaginary parts of the dielectric constant of gold, respectively, ϵ_∞ is the dielectric background, $\omega_p = \sqrt{Ne^2/(\epsilon_0 m^*)}$ is the plasma frequency, N is the free electron density, e is the elementary charge, ϵ_0 is the permittivity of vacuum, m^* is the effective mass of the electron, $\omega_\tau = 1/\tau$ is the electron scattering rate, and τ is the electron scattering time.

Considering only non-radiative losses, the SPP propagation length L_{SPP} at the gold/air interface is expressed as

$$L_{\mathrm{SPP}} = \frac{1}{2\,\mathrm{Im}[k_{\mathrm{SPP}}]}, \qquad (3)$$

where $k_{\mathrm{SPP}} = (\omega/c)\sqrt{\tilde{\epsilon}/(\tilde{\epsilon}+1)}$ is the complex wavenumber of SPP and c is the speed of light in vacuum. By substituting the dielectric constant of polycrystalline gold[27] into Eq. (3), L_{SPP} is calculated to be 12.3 mm at a wavelength of 10.6 μm. Our experimentally measured values of 9.0 ± 0.3 mm, 12.0 ± 0.4 mm, and 14.7 ± 0.7 mm agree with this theoretical estimation, confirming that mid-IR SPPs at the gold/air interface propagate for a distance about or above 10 mm. This agreement suggests that non-radiative losses have major contribution to the observed attenuation behavior.

Assuming $\epsilon'' < |\epsilon'|$ and $|\epsilon'| \gg 1$, both of which are valid for $\omega_\tau < \omega \ll \omega_p$, Eq. (3) is approximated as[28]

$$L_{\mathrm{SPP}} \simeq \frac{c}{\omega}\left(\frac{\epsilon'+1}{\epsilon'}\right)^{3/2}\frac{\epsilon'^2}{\epsilon''} \simeq \frac{c}{\omega}\frac{\epsilon'^2}{\epsilon''}. \qquad (4)$$

Here, we note that our operating frequency $\omega \sim 1/5.6\,\mathrm{fs}^{-1}$, corresponding to 943 cm^{-1} in wavenumber, satisfies the condition $\omega_\tau < \omega \ll \omega_p$, according to the spectroscopic ellipsometry measurements on evaporated gold[20,21] (e.g., the scattering rate ω_τ is $<1/14\,\mathrm{fs}^{-1}$, or $<380\,\mathrm{cm}^{-1}$, for grain size of >56 nm,[21] and the plasma frequency ω_p exists in the ultraviolet region). Equation (4) describes how L_{SPP} depends on ϵ' and ϵ'', and therefore on the Drude parameters of ω_τ, ϵ_∞, and ω_p.

Trollmann and Pucci[21] have evaluated the Drude parameters for evaporated gold films of varied morphology. They have shown that the electron scattering rate ω_τ increases with decreasing grain size, and that such dependence becomes even stronger when the grain size is smaller than their estimated bulk electron mean free path of ~56 nm. Here, we note that their estimated value is compatible with the value 35.9 nm measured for single crystalline gold by Canchal-Arias and Dawson[29] According to the results of Trollmann and Pucci,[21] the electron scattering rate of our twice-annealed sample (the grain size of 2000 nm) is about 1.5 times smaller than that of our as-grown sample (the grain size of 70 nm). Now, it is reasonable to interpret our results as that thermal annealing induced the grain-size enlargement, and the accompanying lowering of ω_τ.

A lowering in ω_τ should result in the elongation of L_{SPP}, as explained in the following. From Eqs. (2) and (4), we obtain:

$$\frac{dL_{SPP}}{d\omega_\tau} \simeq \frac{c}{\omega}\frac{\epsilon'}{\epsilon''^2}\left(2\frac{d\epsilon'}{d\omega_\tau}\epsilon'' - \epsilon'\frac{d\epsilon''}{d\omega_\tau}\right) \simeq \frac{c}{\omega^2}\frac{\epsilon'}{\epsilon''^2}\frac{\omega_p^4\left(\omega^2+3\omega_\tau^2\right)}{\left(\omega^2+\omega_\tau^2\right)^3}, \tag{5}$$

where $\epsilon' \simeq -\omega_p^2/(\omega^2+\omega_\tau^2)$ is used to derive the final expression. Since $\epsilon' < 0$ holds at our operating frequency ω, we obtain $dL_{SPP}/d\omega_\tau < 0$. There are two kinds of physics behind the behavior that L_{SPP} monotonically elongates with decreasing ω_τ. One is the suppression in local Joule heating efficiency, expressed as a decrease in ϵ''. The other is that increased portion of the electromagnetic field exists in air (outside gold), which suppresses the total Ohmic losses.

For quantitative understanding of SPP attenuation in visible range, Kuttge *et al.*[12] studied additional loss mechanism, namely, scattering of SPPs at grain boundaries, by measuring both the propagation length and the dielectric function. Lee *et al.*[30] showed the existence of electromagnetic hotspots on copper films owing to multiple SPP reflection within the hotspots or cavity effect, and associated them with triple junctions, where three grain boundaries intersect on the surface, and large and deep boundary grooves. Our observation of elongated L_{SPP} with enlarged grain size is in line with their conclusions that grain boundaries induce SPP attenuation.

Suppressed surface roughness may also lead to elongated L_{SPP} by reducing the scattering of SPPs. This contribution, however, would be negligible in our observed elongation of L_{SPP}, since attenuation due to SPP scattering by surface roughness of <10 nm is estimated to be by many orders of magnitude smaller than the attenuation for the propagation length of ~10 mm.[12,19,31]

Based on the discussions above, we attribute the elongation of SPP propagation length to suppressed non-radiative damping (or Ohmic loss) and suppressed SPP scattering, both of which originate from reduction in grain boundaries. Simultaneous measurements on dielectric constants would enable us to distinguish one contribution from another.

We lastly comment on the phenomena induced by the thermal annealing. Observed enlargement of the grain size is understood as a result that smaller crystallite grains preferentially melt upon annealing[32] and re-crystallize into larger particles. During such phenomena, each crystallite grain can be connected with each other by the necking formation, which would suppress the surface roughness and make grain boundaries invisible with AFM. The minor side effect of annealing was the formation of pinholes with diameters on the order of 100 nm at the metal surface. They appeared with a number density of 0.16 μm^{-2} after the first annealing and with a number density of 0.44 μm^{-2} after the second annealing. Such pinholes are much smaller than the SPP wavelength but may have induced scattering of SPPs and reduced the net elongation of L_{SPP}.

VI. CONCLUSIONS

We demonstrated that SPPs at the gold/air interface propagate for a distance about or above 10 mm at a wavelength of 10.6 μm. The measured propagation length is in good agreement with the value predicted from the dielectric constant of polycrystalline gold. We also successfully demonstrated that the SPP propagation length can be increased by the simple treatment of thermal annealing accompanied by the increased grain size and decreased surface roughness. We attributed the elongated propagation length to suppressed non-radiative damping (or Ohmic loss) and suppressed SPP scattering, both of which originate from reduction in grain boundaries. Quantitative evaluation of the SPP propagation length, correlated with material's morphology, is important in designing plasmonic devices and beneficial for deeper understandings of the mechanism of the losses that underlie electric-field enhancement achievable upon SP excitations.

ACKNOWLEDGMENTS

The authors thank K. Hirakawa and K. Yoshida (Institute of Industrial Science, the University of Tokyo: IIS-UTokyo) for technical supports in thermal evaporation and thermal annealing; T. Takahashi and Y. Shimada (IIS-UTokyo) for technical supports in AFM measurements; M. Maeda, H. Kimura, T. Yoshikawa, and T. Narumi (IIS-UTokyo) for technical supports in SEM/EBSD measurements; and K. Edagawa (IIS-UTokyo) for fruitful discussions on materials' morphology. The sample was fabricated at VLSI Design and Education Center (VDEC), the University of Tokyo. Financial support by the Japan Society for the Promotion of Science (MEXT KAKENHI 16K13694) is gratefully acknowledged.

[1]R. Stanley, Nat. Photonics **6**, 409 (2012).
[2]S. Law, V. Podolskiy, and D. Wasserman, Nanophotonics **2**, 103 (2013).
[3]F. Neubrech, A. Pucci, T. W. Cornelius, S. Karim, A. García-Etxarri, and J. Aizpurua, Phys. Rev. Lett. **101**, 157403 (2008).
[4]C. V. Hoang, M. Oyama, O. Saito, M. Aono, and T. Nagao, Sci. Rep. **3**, 1175 (2013).
[5]J. Cleary, R. Peale, D. Shelton, G. Boreman, R. Soref, and W. Buchwald, MRS Proc. **1133**, AA10–03 (~~2011~~). 2008 AQ2
[6]F. Kusunoki, J. Takahara, and I. Kobayashi, Electron. Lett. **39**, 23 (2003).
[7]T. W. Ebbesen, C. Genet, and S. I. Bozhevolnyi, Phys. Today **61**(5), 44 (2008).
[8]R. Soref, R. E. Peale, and W. Buchwald, Opt. Express **16**, 6507 (2008).
[9]F. Kusa, K. E. Echternkamp, G. Herink, C. Ropers, and S. Ashihara, AIP Adv. **5**, 077138 (2015).
[10]F. Kusa and S. Ashihara, J. Appl. Phys. **116**, 153103 (2014).
[11]A. V. Zayats, Nature **495**, S7 (2013).
[12]M. Kuttge, E. J. R. Vesseur, J. Verhoeven, H. J. Lezec, H. A. Atwater, and A. Polman, Appl. Phys. Lett. **93**, 113110 (2008).

[13]R. E. Peale, O. Lopatiuk, J. Cleary, S. Santos, J. Henderson, D. Clark, L. Chernyak, T. A. Winningham, E. D. Barco, H. Heinrich, and W. R. Buchwald, J. Opt. Soc. Am. B **25**, 1708 (2008).

[14]H. U. Yang, J. D'Archangel, M. L. Sundheimer, E. Tucker, G. D. Boreman, and M. B. Raschke, Phys. Rev. B **91**, 235137 (2015).

[15]J. McMullen, Solid State Commun. **17**, 331 (1975).

[16]Z. Schlesinger and A. Sievers, Solid State Commun. **43**, 671 (1982).

[17]Z. Schlesinger and A. J. Sievers, Phys. Rev. B **26**, 6444 (1982).

[18]J. Schoenwald, E. Burstein, and J. Elson, Solid State Commun. **12**, 185 (1973).

[19]H. Shiba, M. Haraguchi, and M. Fukui, J. Phys. Soc. Jpn. **63**, 1400 (1994).

[20]R. L. Olmon, B. Slovick, T. W. Johnson, D. Shelton, S.-H. Oh, G. D. Boreman, and M. B. Raschke, Phys. Rev. B **86**, 235147 (2012).

[21]J. Trollmann and A. Pucci, J. Phys. Chem. C **118**, 15011 (2014).

[22]S. T. Koev, A. Agrawal, H. J. Lezec, and V. A. Aksyuk, Plasmonics **7**, 269 (2012).

[23]J. W. Cleary, G. Medhi, R. E. Peale, and W. R. Buchwald, Appl. Opt. **49**, 3102 (2010).

[24]M. G. Moharam and T. K. Gaylord, J. Opt. Soc. Am. **71**, 811 (1981).

[25]C. Nogues and M. Wanunu, Surf. Sci. **573**, L383 (2004).

[26]P. Klapetek, I. Ohlídal, A. Montaigne-Ramil, A. Bonanni, D. Stifter, and H. Sitter, Acta Phys. Slov. **53**, 223 (2003).

[27]E. D. Palik, *Handbook of Optical Constants of Solids* (Academic Press, 2002).

[28]H. Raether, *Surface Plasmons on Smooth and Rough Surfaces and on Gratings* (Springer, Berlin, 1998).

[29]D. Canchal-Arias and P. Dawson, Surf. Sci. **577**, 95 (2005).

[30]H. S. Lee, C. Awada, S. Boutami, F. Charra, L. Douillard, and R. E. de Lamaestre, Opt. Express **20**, 8974 (2012).

[31]D. L. Mills, Phys. Rev. B **12**, 4036 (1975).

[32]P. Buffat and J.-P. Borel, Phys. Rev. A **13**, 2287 (1976).

D. Franta,